THEORY OF MINERALS AT HIGH AND ULTRAHIGH PRESSURES : STRUCTURE, PROPERTIES, DYNAMICS, AND PHASE TRANSITIONS

A.R. OGANOV
Laboratory of Crystallography, Department of Materials,
ETH Zurich, CH-8092 Zurich, Switzerland

1. Introduction

The interest in minerals at extreme conditions is natural: most of the Earth's interior exists at high pressures (up to 364 GPa) and temperatures (up to ~6000 K). Studying the behaviour, properties, and structure of Earth-forming materials at such conditions allows one to understand better the properties of the Earth's interior and provides clues to important geological problems. Experimental studies are often problematic at such conditions, and theory often provides the only possible route for such studies. Unlike experiment, theory meets no major challenge at extreme conditions, and a single calculation or a series of calculations can provide a wealth of information on many properties of the material. It is fortunate that state-of-the-art quantum-mechanical calculations can provide sufficient accuracy for solving many geologically important problems.

This Chapter is divided into three main parts:

(a) Methodology, where a brief discussion of theoretical methods is given, with a number of references for the interested reader;
(b) Examples from recent studies, which show the power (and limitations) of such calculations;
(c) Discussion.

2. Methodology

The central quantity in any theoretical calculations, either based on quantum mechanics or on simple atomistic models, is the energy. Minimising the total energy with respect to structural parameters, one obtains the optimal theoretical structure. First derivatives of the energy determine forces on atoms, pressure, and stresses. A great number of physical properties can be described in terms of the total energy. For instance, its second derivatives with respect to atomic displacements and strains yield vibrational frequencies and the elastic constants, respectively.

From statistical mechanics, knowing the energy of different states of the system (i.e. the energies of different vibrational and electronic quantum levels or of different atomic configurations) one can calculate the entropy and the free energy[1], the link being provided by the partition function $Z = \sum_i e^{-E_i / k_B T}$. Because of this central role of the total energy, here we will concentrate on general aspects of quantum-mechanical calculations of the total energy.

Quantum non-relativistic[2] systems are described by the Schrödinger equation:

$$\hat{\mathbf{H}} \psi = E\psi \tag{1}$$

where $\hat{\mathbf{H}}$ is the Hamilton operator, E is the total energy, and ψ the wavefunction. Decomposing the Hamiltonian into separate contributions, we write in atomic units:

$$(-\frac{1}{2} \nabla^2 + V_{n\text{-}n} + \hat{V}_{n-e} + \hat{V}_{Hartree} + \hat{V}_{xc})\psi = E\psi \tag{2}$$

where the first term in parentheses is the electronic kinetic energy operator (electrons, being quantum particles, have a kinetic energy even at 0 K!), the second is the nuclear-nuclear electrostatic energy, the third is the electron-nuclear potential energy operator. The fourth term (Hartree potential) is in fact the simplest approximation to the electron-electron potential energy operator, being simply the Coulombic self-energy operator of the electron density distribution $\rho(\mathbf{r})$:

$$V_{Hartree}(\mathbf{r}) = \int \frac{\rho(\mathbf{r}')}{|\mathbf{r} - \mathbf{r}'|} d\mathbf{r}' \tag{3}$$

The final, fifth, operator is the exchange-correlation potential. The main problems in solving the Schrödinger equation are related to: 1) an exceedingly complicated nature of the many-body wavefunction ψ (and, hence, the electronic kinetic energy) and 2) problems in realistic representation of the exchange-correlation energy. All the other terms – the nuclear-nuclear, nuclear-electronic, and Hartree energy – are trivial.

2.1. WAVEFUNCTION, ORBITALS, ELECTRONIC KINETIC ENERGY

The wavefunction, according to the Pauli principle, must be antisymmetric with respect

---

[1] In practical calculations, thermodynamic properties of solids can be obtained from phonon frequencies in the quasiharmonic approximation (see [1] for a review of phonon calculations based on density functional theory). Alternatively, one can extract thermodynamic information from *ab initio* molecular dynamics [2] using thermodynamic integration methods (see, e.g., [3] and [4]) or thermodynamic perturbation theory [5]. Unlike the quasiharmonic approximation, such methods can also be applied to fluids, but one needs to have a good reference model with known free energy (e.g., Lennard-Jones solid or liquid – but such models are of limited applicability).

[2] Relativistic effects become important in heavy elements, where electrons close to the nucleus move at speeds comparable to the speed of light. These effects result in shrinking of the core orbitals, which has indirect effects also on the valence orbitals and on the chemical properties of atoms. Another type of relativistic effects is spin-orbit coupling. Relativistic effects are important only for elements heavier than Kr; their importance becomes crucial for late rare-earth and heavier elements. Treatment of relativistic effects requires solving the Dirac (rather than Schrödinger) or analogous equations.

to the interchange of the electrons; the square of its modulus gives the electron density at each point of space. In most practical calculations the many-body wavefunction is represented via one-electron orbitals, and the simplest antisymmetric wavefunction is a single determinant. The single-determinant representation is used in the Hartree-Fock approximation and in Kohn-Sham density functional theory (in the latter this is not of much importance as the wavefunction is only a means to calculate the electronic kinetic energy). The exact many-body wavefunction can be rigorously represented as a linear combination of determinants composed of the occupied and empty orbitals (this fact is employed in configuration interaction methods, which, however, can be used only for small molecules and not for solids).

The individual one-electron orbitals in crystals (crystal orbitals) obey the Bloch theorem:

$$\phi_{i\mathbf{k}}(\mathbf{r}) = e^{i\mathbf{k}\mathbf{r}} \sum_{\mathbf{G}} C_{\mathbf{k}+\mathbf{G}} \; e^{i\mathbf{G}\mathbf{r}} \quad , \tag{4}$$

which states that each orbital corresponding to a wavevector $\mathbf{k}$ in the Brillouin zone can be represented as a product of a lattice-periodic function (which in Eq. (4) is represented as a Fourier series) and the modulating function $e^{i\mathbf{k}\mathbf{r}}$. Accurate calculations must include a sufficient number of $\mathbf{k}$-points, which can be quite large for metals and small unit cells (also at high pressures). Plane-wave expansion with coefficients $C_{\mathbf{k}+\mathbf{G}}$ as variable parameters is mathematically the most natural way to represent crystal orbitals avoiding any assumptions as to the shape of the orbitals. It is straightforward to achieve basis set completeness in plane-wave calculations. Computations of many properties are practically more convenient in the plane-wave basis set, but the drawback is that an enormous number of plane waves would be necessary to represent the rapidly varying wavefunctions, especially for very compact core orbitals. For this reason, in plane wave calculations core orbitals are either excluded from explicit consideration (their effect on the valence electrons in such cases is represented by an effective core pseudopotential) or treated separately in a non-planewave fashion (in such methods as PAW, APW, LAPW and APW+lo – see, e.g., [6-8] for discussion). Performance of pseudopotentials is usually very good, however it always has to be tested against all-electron calculations. The accuracy of pseudopotential calculations degrades at ultrahigh pressures when core electrons begin to participate directly in interatomic interactions. The main reason to use pseudopotentials is that their use significantly simplifies calculations and still provides accurate results. However, the recently formulated projector augmented-wave method ([7] and [8]), which is an all-electron frozen-core method, enables higher accuracy and even greater computational efficiency.

In an alternative approach both core and valence orbitals are represented as a linear combination of (localised) atomic orbitals (LCAO), whose radial part is described by either Slater or (usually) Gaussian functions, and the angular part is given by spherical harmonics. The number of localised basis functions sufficient for good calculations is usually not too big (except in metals), but it is much more difficult to operate with such functions and achieving basis set completeness is not anymore trivial.
The total kinetic energy and electron density are calculated as sums over occupied orbitals:

$$E_{\text{kin,e}} = \sum_{i,\mathbf{k}} \left\langle \phi_{i\mathbf{k}} \mid -\frac{1}{2}\nabla^2 \mid \phi_{i\mathbf{k}} \right\rangle \qquad (5)$$

$$\rho(\mathbf{r}) = \sum_{i,\mathbf{k}} \mid \phi_{i\mathbf{k}}(\mathbf{r}) \mid^2 \qquad (6)$$

2.2 HARTREE-FOCK APPROXIMATION

The basic assumption of this approximation is that the motions of electrons having opposite spins are totally uncorrelated. For each orbital the Hartree-Fock equations take the form:

$\varepsilon_{i\mathbf{k}}\phi_{i\mathbf{k}}(\mathbf{r}) =$

$$= \{-\frac{1}{2}\nabla^2 + \hat{V}_{n-e}(\mathbf{r}) + \int\frac{\rho(\mathbf{r'})}{|\mathbf{r}-\mathbf{r'}|}d\mathbf{r'}\}\phi_{i\mathbf{k}}(\mathbf{r}) - \sum_{j}\delta_{\sigma_i,\sigma_j}\int d\mathbf{r'}\frac{\phi_{j\mathbf{k}}^*(\mathbf{r'})\phi_{i\mathbf{k}}(\mathbf{r'})}{|\mathbf{r}-\mathbf{r'}|}\phi_{j\mathbf{k}}(\mathbf{r}) , \quad (7)$$

where the last term is the so-called exchange operator, the origin of which is in the Pauli principle, and which does not allow two electrons with the same spin to be found at the same point of space. By definition Hartree-Fock exchange is exact, whereas all the unaccounted effects are known as *electron correlation*. The exact exchange, as seen from Eq. (7), is non-local, i.e. in order to estimate it at a given point of space, information about the wavefunction at all points of space is needed. Electron correlation energy, although much smaller than exchange energy, is very important for chemical bonding, the fact which limits the accuracy of the Hartree-Fock approximation. Because of the nature of electron correlation, the most noticeable errors of this method are related to processes associated with breaking of electron pairs – for instance, chemical bond energies, which are underestimated typically by 30-50%. Considering other properties, this approximation performs reasonably well for ionic crystals, less well for semiconductors, and quite badly for metals.

2.3 DENSITY FUNCTIONAL THEORY (DFT)

It has been proven by Hohenberg & Kohn [9] that electron density distribution $\rho(\mathbf{r})$ uniquely defines the total energy of a material, via a universal functional F[ρ]. In principle, all ground-state properties could then be calculated from only $\rho(\mathbf{r})$. This means that the wavefunction is sufficient, but not necessary for quantum-mechanical description of ground-state properties. Unfortunately, the universal functional F[ρ] is unknown. The main problem here is the kinetic energy, which for atomic systems cannot be reasonably approximated by electron-gas expressions or their extensions. The errors of such expressions are so bad that they do not reproduce, for example, the shell structure of atoms. Up to know, no satisfactory ways of calculating the electronic kinetic energy from the electron density alone have been found.

   In the method of Kohn and Sham [10], this difficulty is overcome by employing a simple single-determinant wavefunction, the only purpose of which is to give a reasonable representation (5) of the kinetic energy. Such a representation is, of course,

not exact, and the difference between the exact and model kinetic energies is put in the exchange-correlation energy, thus making this theory formally exact. In practice, one has to use some approximation for the exchange-correlation energy – such as the local density approximation (LDA: [11-15]), generalised gradient approximation (GGA: e.g., [16] and [17]), or meta-GGA (e.g., [18]). A good discussion of different approximate exchange-correlation functionals can be found in [19] and [20].

Because both the LDA and GGA exchange-correlation functionals are local, i.e. at a given point in space they depend only on the density (for the GGA also on its gradient) at the same point, DFT calculations are much easier compared to Hartree-Fock calculations (where exchange potential is non-local and very complicated – see Eq. (7) above). At the same time, they are usually much more accurate and enable one to study metals.

Both DFT and Hartree-Fock methods do not give accurate band structures – in particular, the band gaps are usually overestimates by a factor of ~2 in the Hartree-Fock approximation and underestimated by a similar factor in DFT calculations. As the wavefunction is only a tool to calculate the electronic kinetic energy in DFT, even if we knew the exact exchange-correlation functional, there would be no guarantee to obtain quantitatively correct band structures. Hartree-Fock approximation, completely missing electron correlation, cannot describe van der Waals bonding; similar difficulties exist for local exchange-correlation functionals as well, although part of dispersion forces is implicitly present even in local DFT approximations.

Tables 1-3 show a comparison of the results of several quantum-mechanical approximate methods with experimental data. Overall, DFT calculations are superior to Hartree-Fock calculations. The relative performance of the LDA and GGA varies from system to system, but overall GGA is better and is applicable to a wider range of problems. Perhaps the most spectacular success of the GGA is for calculations of the atomisation energy, which is ~30-50% overestimated by the LDA and underestimated by a similar amount by Hartree-Fock, whereas the GGA gives values close to experimental (Tables II and III).

TABLE I. Total energies of selected atoms (in a.u.).

Atom	Hartree-Fock	LDA	GGA	Experiment
H	-0.500	-0.479	-0.500	-0.500
He	-2.86	-2.835	-2.900	-2.904
Ne	-128.55	-128.228	-128.947	-128.937
Ar	-526.82	-525.938	-527.539	-527.60

Data were taken from [12], [21], [22].

TABLE II. Atomisation energies of selected molecules (in a.u.).

Molecule	Hartree-Fock	LDA	GGA	Experiment
H_2	3.64	4.90	4.55	4.73
OH	2.95	5.38	4.77	4.64
H_2O	6.72	11.58	10.15	10.06
N_2	4.99	11.58	10.54	9.93
O_2	1.43	7.59	6.24	5.25
CH_4	14.22	20.03	18.21	18.17

Data were taken from [17].

TABLE III. Properties of selected crystals.

Property	Hartree-Fock	LDA	GGA	Experiment
		Diamond (C)		
a, Å	3.58	3.53	3.57	3.567
K_0, GPa	471	455	438	442
E_{at}, eV	-5.2	-8.87	-7.72	-7.55
		Periclase (MgO)		
a, Å	4.191	4.160	4.244	4.20
K_0, GPa	186	198	157	167
E_{at}, eV	-7.32	-	-	-10.28
		Ferromagnetic bcc Fe		
V, Å^3	-	10.44	11.34	11.77
K_0, GPa	-	260	200	172
K_0'	-	4.6	4.5	5.0

Data were taken from [22-25].

3.   Results for Some Important Minerals

3.1. PERICLASE (MgO)

Detailed theoretical studies of MgO, an apparently simple mineral, both chemically and structurally, have revealed rather rich physics. At ambient conditions MgO crystallises in the NaCl structure type ("B1" structure). This structure is extraordinarily stable – in fact, only this structure has ever been observed experimentally, although experiments have explored pressures up to 227 GPa [26] and to the melting temperature. It is expected that under pressure the CsCl-type ("B2") structure will become stable, but the best theoretical calculations [27-31] indicate that the pressure of such a transition is very high, ~510 GPa.

A summary of the calculated properties (unit cell parameter and volume, bulk modulus and its first and second pressure derivatives, B1-B2 transition pressure, high-frequency and static dielectric constants, heat capacity, and entropy) of MgO in comparison with experiment is given in Table 4. The overall agreement is rather good.

For a cubic crystal with all atoms occupying centrosymmetric positions, the elastic constants will obey the Cauchy law ($C_{12}=C_{44}+2P$, where P is the pressure) if interatomic forces are central and pairwise. Both from theory and experiment, MgO has a very large deviation from the Cauchy law. This indicates the importance of many-body interactions in this seemingly simple material. Such interactions, in the first approximation describable, e.g., by the breathing shell model, should be significant in all ionic oxides and silicates.

MgO is also characterised by an unusually high elastic anisotropy; Karki *et al.* [37] were the first to predict a change of the sign of this anisotropy under pressure. At pressures corresponding to the bottom of the lower mantle MgO is perhaps the most elastically anisotropic mantle-forming material. Later, using quasiharmonic calculations based on density-functional perturbation theory, Karki *et al.* [32-33] showed that this conclusion is not changed by thermal effects. This conclusion was also supported by recent all-electron calculations [31]. However, one still needs to explore the effects of Fe impurities on the elastic constants and elastic anisotropy.

TABLE IV. Calculated and measured physical properties of MgO (B1 structure).

Properties	LDA (a)	LDA (b)	LDA (c)	GGA (d)	Experiment
a_0, Å	4.240	4.222	4.167	4.253	4.212
V_0, Å^3	76.2	75.2	72.4	77.0	74.7 [e]
K_0, GPa	172.6	159	172	150.6	160.2 [e]
K_0'	4.004	4.30	4.09	4.103	3.99 [e]
K_0'', GPa^{-1}	-0.025	-0.030	(-0.023)	(-0.027)	(-0.024) [e]
P_{tr} (B1-B2), GPa	490	-	510	509	>227
ε_∞	3.15	3.10	-	-	2.95
ε_0	8.87	-	-	-	9.64 [f]
C_V (300 K), Jmol^{-1}K^{-1}	36.58 [h]	36.54 [h]	-	-	36.87 [g]
S (300 K), Jmol^{-1}K^{-1}	26.81	26.65	-	-	27.13 [g]

Equation of state was fitted to the third- or fourth-order Birch-Murnaghan forms (K_0'' given in parentheses indicates the value from the third-order Birch-Murnaghan equation). All theoretical results, except (b), are for the athermally optimised structures. Reference (b) and experimental values are at P=0 and T=300 K.

(a)   [30]. LDA + pseudopotentials.
(b)   [32] and [33]. LDA + pseudopotentials.
(c)   [27]. All-electron (LAPW) LDA calculations.
(d)   [31]. All-electron (PAW) GGA calculations.
(e)   Experimental data [34].
(f)   Experimental data [35] at 300 K. At 0 K ε_0=9.34.
(g)   Experimental data [36]. For calculations [32-33] and experimental data C_V was recalculated from the published C_P using $C_P=C_V(1+\alpha\gamma T)$ and published thermal expansion and Grüneisen parameters.

The B1-B2 phase boundary has been calculated in [38], [39], and [30]. The work [30] was the first fully *ab initio* calculation of this boundary; the results are in better agreement with [38] than with [39]. The phase diagram was calculated in the quasiharmonic approximation, using density-functional perturbation theory (see [1]) to get the phonon spectra, and is shown in Fig. 1. As is clear from this phase diagram, at all conditions present within the Earth MgO is stable only in the NaCl ("B1") structure.

These lattice-dynamical calculations [30] have provided some additional insight. For example, zero-point vibrations were found to lower the B1-B2 transition pressure by 16 GPa. This effect is often neglected in theoretical calculations, but in this case it is larger than usual. The quality of the calculations can be seen from the comparison of the experimental and theoretical phonon dispersion curves (Fig. 2). According to the calculations, B2 phase is dynamically unstable at all pressures below 110 GPa. This means that this phase, when synthesised in its stability field, can only be decompressed to no lower than 110 GPa – at lower pressures it would spontaneously transform into another (probably, the B1) phase.

At ultrahigh pressures, the B2 phase was found to undergo metallization at 20.7 TPa [30]. This is well above the pressure range found within any of the planets. The metallization itself is related to band broadening and overlap between the valence and conduction bands under ultrahigh pressure. Such insulator-metal transitions play an important role in planetary physics. For instance, the magnetic field in Jupiter is almost entirely due to metallization of fluid hydrogen in its interior. MgO provides one of the simplest model materials for studies of such transitions (although in case of fluids there will be additional important effects related to thermal disorder).
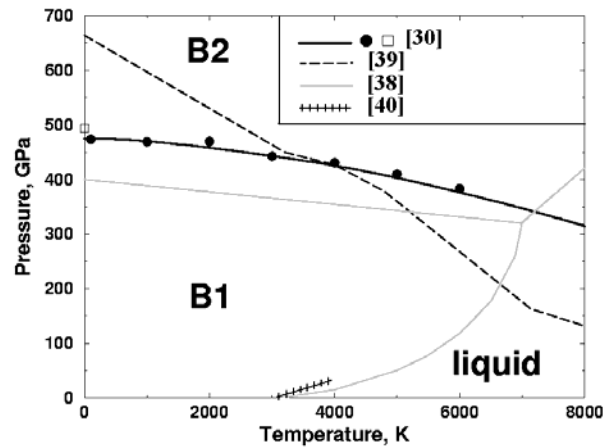
Figure 1. Phase diagram of MgO (from [30]). Calculations of Oganov *et al.* [30]: *solid black line* – result of integration of the Clapeyron slopes, *solid circles* – direct calculations, *open square* – static transition pressure. These calculations utilised the LDA and pseudopotentials. Other symbols are explained in the legend. The experimental melting curve [40] does not agree with theoretical calculations [38] and more recent *ab initio*-based calculations (P. Tangney & S. Scandolo, *pers. comm.*)
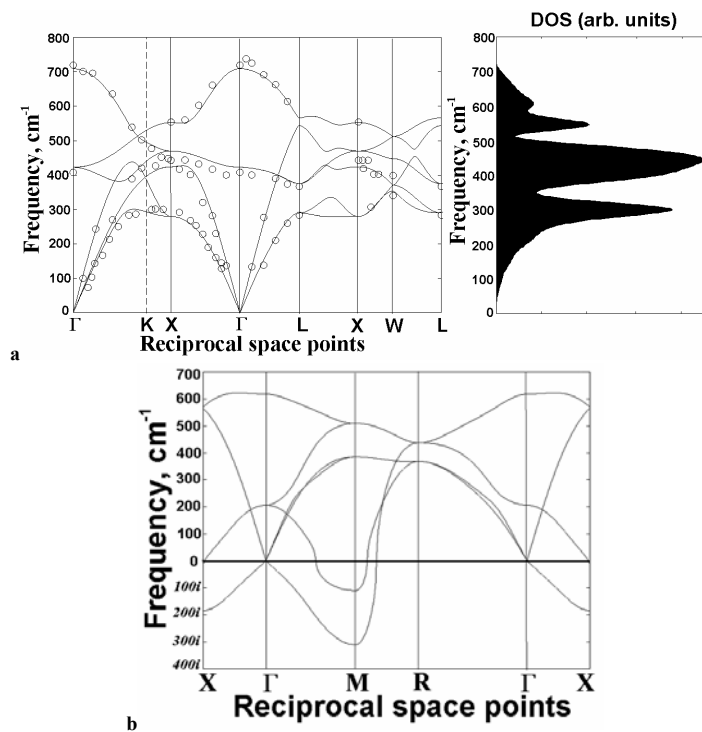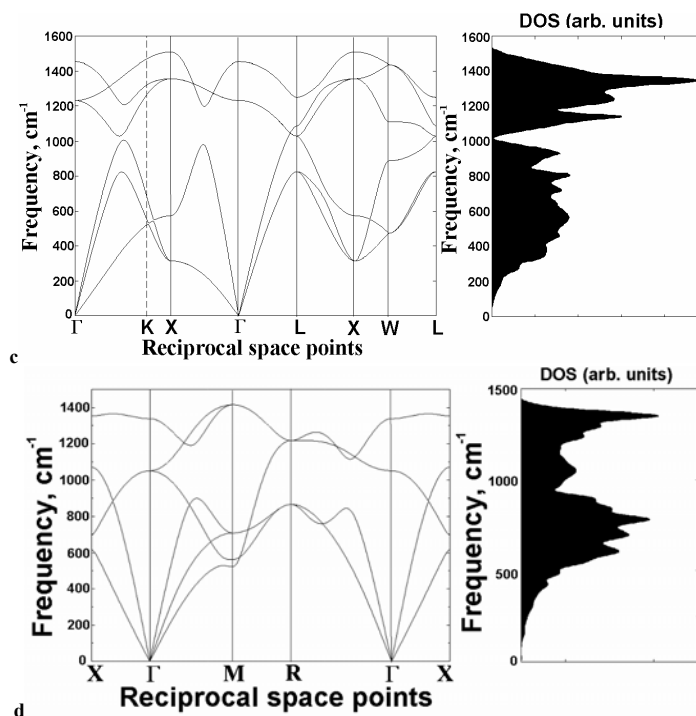
Figure 2. Phonon dispersion curves at 0 GPa in (a) B1-structured and (b) B2-structured MgO and at 600 GPa in (c) B1 phase and (d) B2 phase. From [30].

3.2. SiO$_2$ POLYMORPHS AT HIGH PRESSURE

There have been a number of important theoretical studies of SiO$_2$ polymorphs, and it is remarkable how closely experimental studies reproduced theoretical predictions. The current picture is that stishovite, a high-pressure rutile-structured phase of silica [41] stable above 8 GPa, at 45-55 GPa becomes mechanically unstable and acquires an orthorhombic distortion [42-53]. This distorted structure is known as the CaCl$_2$-type structure. This transition is considered as a classical second-order transition ([44], [51], [52]), although some doubts have been expressed [53]. At 80-100 GPa the α-PbO$_2$ structure becomes stable ([44], [45], [46], [49], [52], [54], [55]). The sequence stishovite - CaCl$_2$ structure - α-PbO$_2$ structure reveals the tendency towards more geometrically regular close packing of the anions. The density differences between these phases are very small. However, according to theoretical predictions ([44], [45], [46], [52]), a phase with the pyrite structure phase becomes thermodynamically stable at 200-220 GPa, and this structure cannot be described as based on a close packing of spherical anions, yet its density is significantly higher (compared with the α-PbO$_2$ structure, its density is 4.6% higher at 0 GPa and 3.2% higher at the transition pressure – [52]). The name "pyrite structure" is rather nominal in this case, and the name "modified pyrite structure" might be more appropriate: the shortest O-O distances are quite long, perhaps too long to be

counted as bonds, 2.361 Å at 0 GPa and 2.047 Å at 260 GPa. Analogous pyrite-type structures have been experimentally found at high pressure in SnO_2, RuO_2, PbO_2 [56] and GeO_2 [57]. Relative enthalpies of different phases are shown in Fig. 3. The calculated crystal structures of the high-pressure SiO_2 polymorphs are shown in Fig. 4.
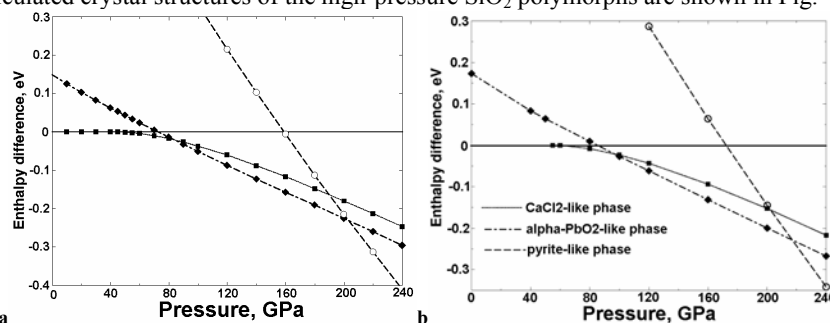

Figure 3. Enthalpy (relative to stishovite, per formula unit) of the high-pressure phases of SiO_2: (a) pseudopotential LDA calculations, (b) all-electron PAW calculations.
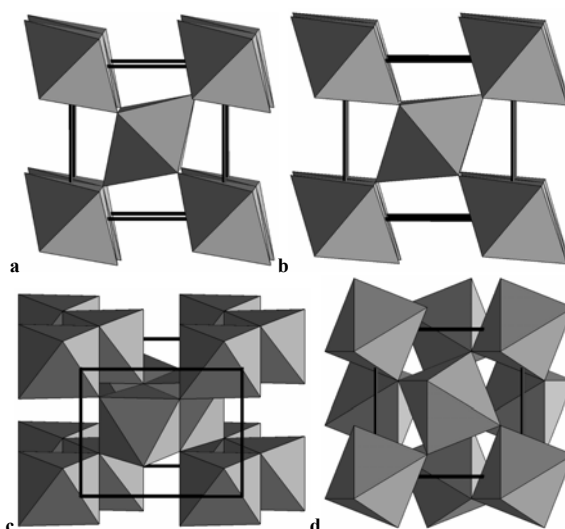

Figure 4. Calculated crystal structures of SiO_2 polymorphs: (a) stishovite at 20 GPa, (b) $CaCl_2$-type phase at 70 GPa, (c) α-PbO_2-type phase at 120 GPa, (d) Pyrite-type phase at 220 GPa.

Applying topological analysis of the total electron density [58] to the pyrite-type SiO_2, one can see [52] that this material is quite ionic (charges of Si atoms at 0 GPa are : +3.23 in stishovite[3], +3.20 in the α-PbO_2-like phase, and +3.17 in the pyrite-type phase) and Si atoms are clearly octahedrally coordinated. One can also see a (3, -1)

---

[3] Kirfel *et al.* [59] found the following Bader charges in stishovite: +3.39 (Si) and -1.69 (O) from experimental charge densities and +3.30 (Si) and -1.65 (O) from GGA calculations (our number were based on LDA densities).

critical point between the nearest O atoms, but a positive Laplacian of the density shows that there is no covalent bond between these atoms, but instead there is a significant closed-shell interaction : $\nabla^2\rho(\text{O-O}) = 3.45$ e Å^{-5} at 0 GPa and 8.26 e Å^{-5} at 260 GPa (for comparison, at the Si-O bond critical point $\nabla^2\rho(\text{Si-O})= 8.12$ and 19.21 e Å^{-5} at 0 GPa and 260 GPa, respectively). Positive Laplacian means that the electron density is depleted (rather than concentrated, as would be the case in covalent bonding) in the interatomic region. Valence electron density also does not show any build-up between the O atoms.

3.3. CORUNDUM (Al$_2$O$_3$)

Both theoretical ([60] and [61]) and experimental [62] work has demonstrated that at 80-100 GPa Al$_2$O$_3$ transforms from the corundum structure into the Rh$_2$O$_3$(II) structure (Fig. 5). This transition, just like the α-PbO$_2$ – pyrite structure transition in SiO$_2$, shows a big departure from a close packed anion arrangement at high pressure.
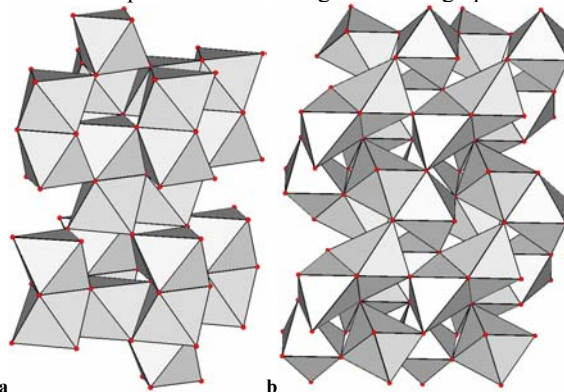

a   **b**
Figure 5. Structure types of (a) corundum and (b) Rh$_2$O$_3$(II).

Close packing can be violated when electronic transitions occur or when coordination numbers of cations become incompatible with close-packed anion arrangements which have only 2-, 3-, 4-, and 6-coordinated sites. However, none of these phenomena take place in SiO$_2$ and Al$_2$O$_3$. One could speculate that in the high-pressure phases of SiO$_2$ and Al$_2$O$_3$ anions are no longer spherical and therefore ideas of close packing of spheres are irrelevant. Irregular shapes of atoms (which can be defined in Bader theory – [58]) are energetically expensive, but can (depending on the structure) result in a higher density – and it is the crystal density that ultimately determines the high-pressure structural stability. Such examples as Al$_2$O$_3$ and SiO$_2$ show the limited applicability of the close packing principle.

3.4. Al$_2$SiO$_5$ POLYMORPHS

The high-pressure stability of the Al$_2$SiO$_5$ polymorphs has been a controversial topic for many years. Ahmed-Zaid and Madon [63-64] claimed to have synthesised a new form of

Al_2SiO_5, with a close-packed V_3O_5-like structure, and suggested it to be the main Al-bearing mineral in the Earth's lower mantle. However, the rest of experimental evidence ([65] and [66]) and theoretical calculations [67] showed that Al_2SiO_5 polymorphs decompose into Al_2O_3 and SiO_2 instead. Good agreement was found between the theoretical decomposition pressure (11 GPa : [67]) and the experimental value of 9.5 GPa [66].

Oganov *et al.* [68] also found that at low temperature the Al_2SiO_5 polymorphs can exist as metastable states up to much higher pressures when transitions into other metastable phases occur. Andalusite was predicted to undergo pressure-induced amorphisation at ~52 GPa and 0 K, whereas sillimanite was predicted to undergo a strongly first-order isosymmetric transition at 37.5 GPa (at somewhat lower pressures and low temperatures an intermediate, incommensurately modulated, phase was also predicted). Both phases have the *Pbnm* space group, but atomic coordination is somewhat different (in the new phase all Si atoms and half of the Al atoms have a 5-fold coordination) – see Fig. 6. It remains to perform experiments to verify these predictions of theory.
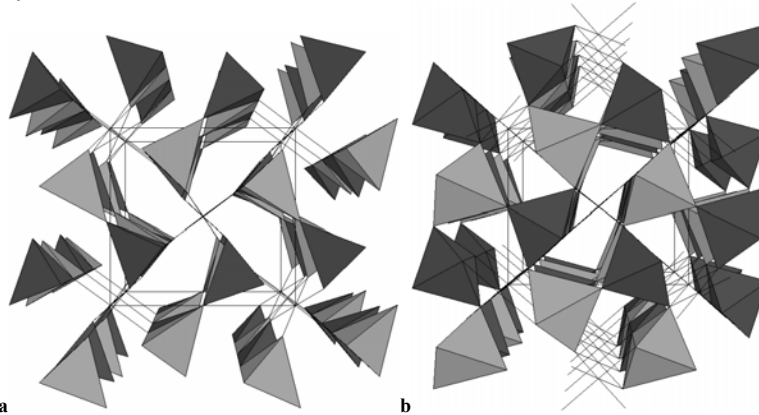

a   **b**

Figure 6. Crystal structure of (a) sillimanite at and (b) isosymmetric meta-sillimanite phase [68].

3.5. MgSiO$_3$ PEROVSKITE

MgSiO$_3$ perovskite, the mineral dominating the composition of the Earth's lower mantle, has been a subject of a number of detailed theoretical and experimental studies. Since the first *ab initio* works on this material [69-72] great progress has been made in theoretical methodology, and many fundamentally important results have been obtained. Both these early works and later investigations ([73, [74], [75]) have confirmed that MgSiO$_3$ perovskite has the *Pbnm* symmetry at all conditions of the Earth's mantle. Although some experimental ([76], [77]) and theoretical [78] evidence has been presented in favour of decomposition of MgSiO$_3$ perovskite into the mixture of MgO and SiO$_2$ at high pressure and temperature, the majority of experimental [79-82] and theoretical ([70], [83]) evidence indicates its stability to decomposition. In fact, theoretical calculations predict an increase of stability of MgSiO$_3$ perovskite relative to

MgO+SiO$_2$ with both pressure (Fig. 7) and temperature [83].

   Detailed calculations of the elastic constants of MgSiO$_3$ perovskite as a function of pressure ([84], [85], [74]) and temperature [75] exist. The agreement with experimental data (elastic constants at 0 GPa [86], and pressure derivatives of the bulk and shear moduli at 0 GPa [87]) is very good. These calculations constitute one of the basic sources of information for interpretations of seismic models of the Earth's lower mantle. The first theoretical determination of the temperature derivatives of seismic wave velocities at lower-mantle pressures and temperatures [75] has also been used for interpreting seismic tomography data in terms of temperature variations in the lower mantle. The results implied a large, ~2000 K temperature difference between the coldest regions of the mantle and the outer core at the core-mantle boundary. With further progress in mineral physics, it will soon be possible to extract also the compositional variations in the Earth's mantle from seismic tomography data.
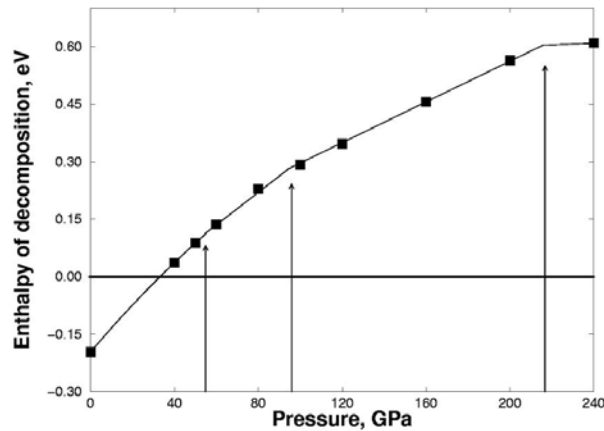

Figure 7. Enthalpy of decomposition of MgSiO$_3$ perovskite calculated at the GGA level of theory [83]. This calculation takes into account phase changes in SiO$_2$ in the considered pressure range – these phase changes are marked by arrows.

4.   Discussion

This chapter presents a brief summary of some of the most popular *ab initio* simulation methods, and their applications to a few important mineral systems. For a more detailed review, the reader is referred to [88]. At present, *ab initio* methods can give reliable qualitative and semiquantitative results for most systems. At high pressures and temperatures, where experiments are very non-trivial, theoretical results may often be superior. For example, experimental determinations of the elastic constants at high pressure are problematic and have large uncertainties. *Ab initio* calculations of the elastic constants of MgO ([37], [31]) agree well with experimental results ([89], [90]) at low pressures, but show significant differences above 20 GPa (experiments went up to 55 GPa [89] and 47 GPa [90]). The accuracy of *ab initio* calculations does not deteriorate with pressure, and one can expect that the main differences are due to non-

hydrostatic conditions of experiments at such pressures. This does not mean, of course, that theory is always right. In certain cases modern theoretical methods meet with serious limitations. The most important of these limitations are the following:

1) The calculated band structure is always very crude: band gaps are typically overestimated by a factor of two by the Hartree-Fock approximation, and underestimated by a factor of two in DFT calculations. This is of no importance for structure and properties in most situations, but for many transition metal oxides (e.g., FeO) DFT (within the LDA and GGA) incorrectly predicts a metallic ground state. This leads to a partial occupation of wrong electronic states and sometimes significant errors in the structure, magnetic moments, phase stability, and physical properties. This also means that insulator-metal transitions can be problematic for theory. Electronic contributions to thermal properties would also be wrong.

To overcome these problems, several methods have been devised, such as the DFT+U method ([91], [92]), SIC-DFT procedures ([12], [93]). Hybrid functionals, such as B3LYP, constructed as a mixture of DFT exchange-correlation and Hartree-Fock exchange [94], also appear to give reasonable electronic structure for such compounds [95]. Meta-GGA functionals ([18], [20]) may be a way forward, but have not yet been systematically applied to transition metal oxides. The GW approximation (see [96]) allows one to get correct electronic structure, but it is not so straightforward to calculate the total energy in this approach. Finally, quantum Monte Carlo methods (see [97]), which are essentially exact stochastic *ab initio* methods, hold a great promise for the future. However, at the moment they are prohibitively expensive for most systems.

2) Van der Waals bonding, originating from dynamical electron correlation, is not well described. Hartree-Fock calculations completely miss this effect. DFT calculations are very crude. Although in some DFT approximations (e.g., [17]) it is often possible to get the correct bond lengths in van der Waals compounds, the energy varies exponentially with distance, instead of the classical R^{-6} dependence.

This problem can, of course, be solved by using quantum Monte Carlo methods, but other methods are emerging as well ([98], [99]). Fortunately, at high pressure the importance of the van der Waals interactions becomes less important relative to other interactions (e.g., exponential interatomic repulsion), and standard DFT calculations, which capture well these repulsions, become accurate at high pressures [100].

5. Acknowledgements

6. References

1. Baroni, S., de Gironcoli, S., Dal Corso, A., Gianozzi, P. (2001) Phonons and related crystal properties from density-functional perturbation theory, *Rev. Mod. Phys.* **73**, 515-562.
2. Car, R. and Parrinello, M. (1985) Unified approach for molecular dynamics and density-functional theory, *Phys. Rev. Lett.* **55**, 2471-2474.
3. Frenkel, D. and Smit, B. (2002) *Understanding Molecular Simulations. From Algorithms to Applications*, Academic Press, San Diego.
4. Sugino, O. & Car, R. (1995) *Ab initio* molecular dynamics study of first-order phase transitions: melting of silicon, *Phys. Rev. Lett.* **74**, 1823-1826.
5. Landau, L.D. and Lifshitz, E.M. (1980) *Statistical Physics.* Part I. (Course of Theoretical Physics, v. 5). Butterworth & Heinemann, Oxford.
6. Singh, D.J. (1994) *Planewaves, Pseudopotentials and the LAPW Method.* Kluwer, Boston.
7. Blöchl, P.E. (1994) Projector augmented-wave method, *Phys. Rev.* **B50**, 17953-17979.
8. Kresse, G. and Joubert, D. (1999) From ultrasoft pseudopotentials to the projector augmented-wave method, *Phys. Rev.* **B59**, 1758-1775.
9. Hohenberg, P. & Kohn, W. (1964) Inhomogeneous electron gas, *Phys. Rev.* **136**, B864-B871.
10. Kohn, W. & Sham, L.J. (1965) Self-consistent equations including exchange and correlation effects, *Phys. Rev.*, **140**, A1133-A1138.
11. Ceperley, D.M. & Alder, B.J. (1980) Ground state of the electron gas by a stochastic method, *Phys. Rev. Lett.* **45**, 566-569.
12. Perdew, J.P. & Zunger, A. (1981) Self-interaction correction to density-functional approximations for many-electron systems, *Phys. Rev.* **B23**, 5048-5079.
13. Vosko, S.H., Wilk, L., Nusair, M. (1980) Accurate spin-dependent electron liquid correlation energies for local spin density calculations: a critical analysis, *Can J. Phys.* **58**, 1200-1211.
14. Perdew, J.P., Wang, Y. (1992) Accurate and simple analytic representation of the electron-gas correlation energy, *Phys. Rev.* **B45**, 13244-13249.
15. Ortiz, G. & Ballone, P. (1994) Correlation energy, structure factor, radial distribution function, and momentum distribution of the spin-polarised uniform electron gas, *Phys. Rev.* **B50**, 1391-1405. (erratum: *Phys. Rev.* **B56** (1997), 970).
16. Wang, Y. & Perdew, J.P. (1991) Correlation hole of the spin-polarized electron gas, with exact small-vector and high-density scaling, *Phys. Rev.* **B44**, 13298-13307.
17. Perdew, J.P., Burke, K., Ernzerhof, M. (1996) Generalized gradient approximation made simple, *Phys. Rev. Lett.* **77**, 3865-3868.
18. Perdew, J.P., Kurth, S., Zupan, A., Blaha, P. (1999) Accurate density functionals with correct formal properties: a step beyond the generalized gradient approximation, *Phys. Rev. Lett.* **82**, 2544-2547.
19. Perdew, J.P., Kurth, S. (1998) Density functionals for non-relativistic Coulomb systems, in D.P. Joubert (ed.), *Density Functionals: Theory and Applications*. Lecture Notes in Physics, v. 500, Springer Verlag, Berlin, pp.8-59.
20. Kurth, S., Perdew, J.P., Blaha, P. (1999) Molecular and solid-state tests of density functional approximations: LSD, GGAs, and meta-GGAs, *Int. J. Quant. Chem.* **75**, 889-909.
21. Parr, R.G. & Yang, W. (1989) *Density-Functional Theory of Atoms and Molecules.* Oxford University Press, Oxford.
22. Lee, I-H. & Martin, R.M. (1997) Applications of the generalised-gradient approximation to atoms, clusters, and solids, *Phys. Rev.* **B56**, 7197-7205.
23. Lichanot, A. (2000) Hartree-Fock and density functional calculations of the elastic constants of the alkaline-earth oxides: comparison with experiment, *Solid State Commun.* **116**, 543-546.
24. Dovesi, R. (1996) Total energy and related properties, in C. Pisani (ed.), *Quantum-mechanical ab intio calculation of the properties of crystalline materials,* Lecture Notes in Chemistry, v. 67, Springer Verlag, Berlin, pp.179-207.
25. Zupan, A., Blaha, P., Schwarz, K., & Perdew, J.P. (1998) Pressure-induced phase transitions in solid Si, SiO$_2$, and Fe: Performance of local-spin-density and generalized-gradient-approximation density functionals, *Phys. Rev.* **B58**, 11266-11272.
26. Duffy, T.S., Hemley, R.J., Mao, H.-K. (1995) Equation of state and shear strength at multimegabar pressures: magnesium oxide to 227 GPa, *Phys. Rev. Lett.* **74**, 1371-1374.
27. Mehl, M.J. and Cohen, R.E. (1988) Linearized augmented plane wave electronic structure calculations for MgO and CaO, *J. Geophys. Res.* **93**, 8009-8022.

28. Habas, M.-P., Dovesi, R., Lichanot, A. (1998) The $B_1 \Leftrightarrow B_2$ phase transition in alkali-earth oxides: a comparison of *ab initio* Hartree-Fock and density functional calculations, *J. Phys.: Condens. Matter* **10**, 6897-6909.

29. Jaffe, J.E., Snyder, J.A., Lin, Z., Hess, A.C. (2000) LDA and GGA calculations for high-pressure phase transitions in ZnO and MgO, *Phys.* Rev. **B62**, 1660-1665.

30. Oganov, A.R., Gillan, M.J., Price, G.D. (2003) *Ab initio* lattice dynamics and structural stability of MgO, *J. Chem. Phys.* **118**, 10174-10182.

31. Oganov, A.R. & Dorogokupets, P.I. (2003) All-electron and pseudopotential study of MgO: Equation of state, anharmonicity, and stability, *Phys. Rev.* **B67**, art. 224110.

32. Karki, B.B., Wentzcovitch, R.M., de Gironcoli, S., & Baroni, S. (1999) First-principles determination of elastic anisotropy and wave velocities of MgO at lower mantle conditions, *Science* **286**, 1705-1707.

33. Karki, B.B., Wentzcovitch, R.M., de Gironcoli, S., & Baroni, S. (2000). High-pressure lattice dynamics and thermoelasticity of MgO, *Phys. Rev.* **B61**, 8793-8800.

34. Speziale, S., Zha, C.-S., Duffy, T.S., Hemley, R.J., Mao, H.-K. (2001) Quasi-hydrostatic compression of magnesium oxide to 52 GPa: Implications of the pressure-volume-temperature equation of state, *J. Geophys. Res.* **B106**, 515-528.

35. Jasperse, J.R., Kahan, A., Plendl, J.N., Mitra, S.S. (1966) Temperature dependence of infrared dispersion in ionic crystals LiF and MgO, *Phys. Rev.* **146**, 526-542.

36. Robie, R.A. & Hemingway, B.S. (1995) *Thermodynamic Properties of Minerals and Related Substances at 289.15 K and 1 bar (10^5 Pascals) Pressure and at Higher Temperatures,* U.S. Geological Survey Bulletin 2131, Washington.

37. Karki, B.B., Stixrude, L., Clark, S.J., Warren, M.C., Ackland, G.J., Crain, J. (1997) Structure and elasticity of MgO at high pressure, *Am. Mineral.* **82**, 51-60.

38. Strachan, A., Çağin, T., Goddard, W.A. III (1999) Phase diagram of MgO from density-functional theory and molecular-dynamics simulations, *Phys. Rev.* **B60**, 15084-15093.

39. Drummond, N.D. & Ackland, G.J. (2002) *Ab initio* quasiharmonic equations of state for dynamically stabilized soft-mode materials, *Phys. Rev.* **B65**, art. 184104.

40. Zerr, A., Boehler, R. (1994) Constraints on the melting temperature of the lower mantle from high-pressure experiments on MgO and magnesiowüstite, *Nature* **371**, 506-508.

41. Stishov, S.M. and Popova, S.V. (1961) New dense polymorphic modification of silica, *Geokhimiya* **10**, 837-839.

42. Kingma, K.J., Cohen, R.E., Hemley, R.J., & Mao, H.-k. (1995) Transformations of stishovite to a denser phase at lower-mantle pressures, *Nature* **374**, 243-245.

43. Lee, C., Gonze, X. (1995) The pressure-induced ferroelastic phase transition of SiO_2 stishovite, *J. Phys. : Condens. Matter* **7**, 3693-3698.

44. Karki, B.B., Warren, M.C., Stixrude, L., Ackland, G.J., & Crain, J. (1997) *Ab initio* studies of high-pressure structural transformations in silica, *Phys. Rev.* **B55**, 3465-3471. (Erratum : *Phys. Rev.* **B56**, 2884).

45. Dubrovinsky, L.S., Saxena, S.K., Lazor, P., Ahuja, R., Eriksson, O., Wills, J.M., Johansson, B. (1997) Experimental and theoretical identification of a new high-pressure phase of silica, *Nature* **388**, 362-365.

46. Teter, D.M., Hemley, R.J., Kresse, G., & Hafner, J. (1998) High pressure polymorphism in silica, *Phys. Rev. Lett.* **80**, 2145-2148.

47. Ono, S., Hirose, K., Murakami, M., Isshiki, M. (2002) Post-stishovite phase boundary in SiO_2 determined by in situ X-ray observations, *Earth Planet. Sci Lett.* **197**, 198-192.

48. Shieh, S.R., Duffy, T.S., Li, B. (2002) Strength and elasticity of SiO_2 across the stishovite-$CaCl_2$-type structural phase boundary, *Phys. Rev. Lett.* **89**, art. 255507.

49. Akins, J.A. and Ahrens, T.J. (2002) Dynamic compression of SiO_2: a new interpretation, *Geophys. Res. Lett.* **29**, art. 10.1029/2002GL014806.

50. Murakami, M., Hirose, K., Ono, S., Ohishi, Y. (2003) Stability of $CaCl_2$-type and alpha-PbO_2-type SiO_2 at high pressure and temperature determined by in-situ X-ray measurements, *Geophys. Res. Lett.* **30**, art. 1207.

51. Andrault, D., Fiquet, G., Guyot, F., Hanfland, M. (1998) Pressure-induced Landau-type transition in stishovite, *Science* **282**, 720-724.

52. Oganov, A.R., Gillan, M.J., Price, G.D. (2003) Structural stability of silica at high pressures and temperatures, *In preparation.*

53. Hemley, R.J., Shu, J., Carpenter, M.A., Hu, J., Mao, H.K., Kingma, K.J. (2000) Strain/order parameter coupling in the ferroelastic transition in dense SiO_2, *Solid State Commun.* **11**, 527-532.

54. Dubrovinsky, L.S., Dubrovinskaya, N.A., Saxena, S.K., Tutti, F., Rekhi, S., LeBihan, T., Shen, G., Hu, J. (2001) Pressure-induced transformations of cristobalite, *Chem. Phys. Lett.* **333**, 264-270.

55. Dubrovinskaia, N.A., Dubrovinsky, L.S., Saxena, S.K., Tutti, F., Rekhi, S., Le Bihan, T. (2001) Direct transition from cristobalite to post-stishovite α-PbO$_2$-like silica phase, *Eur. J. Mineral.* **13**, 479-483.

56. Haines, J., Leger, J.M., Schulte, O. (1996) $Pa\overline{3}$ modified fluorite-type structures in metal dioxides at high pressure, *Science* **271**, 629-631.

57. Ono, S., Hirose, K., Isshiki, M., Ohishi, Y. (2003) A new high-pressure form of germanium dioxide, *Phys. Rev. Lett.*, submitted.

58. Bader, R.F.W. (1990) *Atoms in Molecules. A Quantum Theory*, Oxford University Press, Oxford.

59. Kirfel, A., Krane, H.-G., Blaha, P., Schwarz, K., Lippmann, T. (2001) Electron-density distribution in stishovite, SiO$_2$: a new high-energy synchrotron-radiation study, *Acta Cryst.* **A57**, 663-677.

60. Marton, F.C. & Cohen, R.E. (1994) Prediction of a high-pressure phase transition in Al$_2$O$_3$, *Am. Mineral.* **79**, 789-792.

61. Duan, W., Wentzcovitch, R.M., & Thomson, K.T. (1998) First-principles study of high-pressure alumina polymorphs, *Phys. Rev.* **B57**, 10363-10369.

62. Funamori, N. & Jeanloz, R. (1997) High-pressure transformation of Al$_2$O$_3$, *Science* **278**, 1109-1111.

63. Ahmed-Zaid, I. & Madon, M. (1991) A high-pressure form of Al$_2$SiO$_5$ as a possible host of aluminium in the lower mantle, *Nature* **353**, 426-428.

64. Ahmed-Zaid, I. & Madon, M. (1995) Electron microscopy of high-pressure phases synthesized from natural garnets in a diamond anvil cell : Implications for the mineralogy of the lower mantle, *Earth Planet. Sci. Lett.* **129**, 233-247.

65. Liu, L.-G. (1974) Disproportionation of kyanite to corundum plus stishovite at high pressure and temperature, *Earth Planet. Sci. Lett.* **24**, 224-228.

66. Schmidt, M.W., Poli, S., Comodi, P., & Zanazzi, P.F. (1997) High-pressure behavior of kyanite: Decomposition of kyanite into stishovite and corundum, *Am. Mineral.* **82**, 460-466.

67. Oganov, A.R. & Brodholt, J.P. (2000) High-pressure phases in the Al$_2$SiO$_5$ system and the problem of Al-phase in Earth's lower mantle: ab initio pseudopotential calculations, *Phys. Chem. Minerals* **27**, 430-439.

68. Oganov, A.R., Price, G.D., Brodholt, J.P. (2001) Theoretical investigation of metastable Al$_2$SiO$_5$ polymorphs, *Acta Crystallogr.* **A57**, 548-557.

69. D'Arco, Ph., Sandrone, G., Dovesi, R., Orlando, R., & Saunders, V.R. (1993) A quantum mechanical study of the perovskite structure type of MgSiO$_3$, *Phys. Chem. Minerals* **20**, 407-414.

70. D'Arco, Ph., Sandrone, G., Dovesi, R., Apra, E., Saunders, V.R. (1994) A quantum-mechanical study of the relative stability under pressure of MgSiO$_3$-ilmenite, MgSiO$_3$-perovskite, and MgO-periclase + SiO$_2$-stishovite assemblage, *Phys. Chem. Minerals* **21**, 285-293.

71. Wentzcovitch, R.M., Martins, J.L., Price, G.D. (1993) *Ab initio* molecular dynamics with variable cell shape: application to MgSiO$_3$, *Phys. Rev. Lett.* **70**, 3947-3950.

72. Stixrude, L. & Cohen, R.E. (1993) Stability of orthorhombic MgSiO$_3$ perovskite in the Earth's lower mantle, *Nature* **364**, 613-616.

73. Warren, M.C. & Ackland, G.J. (1996) *Ab initio* studies of structural instabilities in magnesium silicate perovskite, *Phys. Chem. Minerals* **23**,107-118.

74. Oganov, A.R., Brodholt, J.P., Price, G.D. (2001) *Ab initio* elasticity and thermal equation of state of MgSiO$_3$ perovskite, *Earth and Planetary Science Letters* **184**, 555-560.

75. Oganov, A.R., Brodholt, J.P., Price, G.D. (2001) The elastic constants of MgSiO$_3$ perovskite at pressures and temperatures of the Earth's mantle, *Nature* **411**, 934-937.

76. Meade, C., Mao, H.K., Hu, J.Z. (1995) High-temperature phase transition and dissociation of (Mg,Fe)SiO$_3$ perovskite at lower mantle pressures, *Science* **268**, 1743-1745.

77. Saxena, S.K., Dubrovinsky, L.S., Lazor, P., Cerenius, Y., Häggkvist, P., Hanfland, M., Hu, J. (1996) Stability of perovskite (MgSiO$_3$) in the Earth's mantle, *Science* **274**, 1357-1359.

78. Dubrovinsky, L.S., Saxena, S.K., Ahuja, R., Johansson, B. (1998) Theoretical study of the stability of MgSiO3-perovskite in the deep mantle, *Geophys. Res. Lett.* **25**, 4253-4256.

79. Serghiou, G., Zerr, A., Boehler, R. (1998) (Mg,Fe)SiO$_3$-perovskite stability under lower mantle conditions, *Science* **280**, 2093-2095.

80. Fiquet, G., Dewaele, A., Andrault, D., Kunz, M., & Le Bihan, T. (2000) Thermoelastic properties and crystal structure of MgSiO$_3$ perovskite at lower mantle pressure and temperature conditions, *Geophys. Res. Lett.* **27**, 21-24.

81. Shim, S.H., Duffy, T.S., Shen, G.Y. (2001) Stability and structure of MgSiO$_3$ perovskite to 2300-kilometer

depth in Earth's mantle, *Science* **293**, 2437-2440.

82. Luo, S.N., Mosenfelder, J.L., Asimow, P.D., Ahrens, T.J. (2002) Direct shock wave loading of Stishovite to 235 GPa: Implications for perovskite stability relative to an oxide assemblage at lower mantle conditions, *Geophys. Res. Lett.* **29**, art. 1691.

83. Oganov, A.R., Price, G.D., Brodholt, J.P. (2003) Theory of $MgSiO_3$ perovskite : from wavefunctions to geophysical implications, *In prep.*

84. Karki, B.B., Stixrude, L., Clark, S.J., Warren, M.C., Ackland, G.J., & Crain, J. (1997) Elastic properties of orthorhombic $MgSiO_3$ perovskite at lower mantle pressures, *Am. Mineral.* **82**, 635-638.

85. Wentzcovitch, R.M., Karki, B.B., Karato, S., & da Silva, C.R.S. (1998) High pressure elastic anisotropy of $MgSiO_3$ perovskite and geophysical implications, *Earth Planet. Sci. Lett.* **164**, 371-378.

86. Yeganeh-Haeri, A. (1994) Synthesis and re-investigation of the elastic properties of single-crystal magnesium silicate perovskite, *Phys. Earth Planet. Inter.* **87**, 111-121.

87. Sinelnikov, Y.D., Chen, G., Neuville, D.R., Vaughan, M.T., & Liebermann, R.C. (1998) Ultrasonic shear wave velocities of $MgSiO_3$ perovskite at 8 GPa and 800 K and lower mantle composition, *Science* **281**, 677-679.

88. Oganov, A.R., Brodholt, J.P., Price, G.D. (2002). *Ab initio* theory of thermoelasticity and phase transitions in minerals, in C.M. Gramaccioli (ed.), *Energy Modelling in Minerals*, EMU Notes in Mineralogy, v.4, Eötvös University Press, Budapest, pp. 83-170.

89. Zha, C.-S., Mao, H.-K., Hemley, R.J. (2000) Elasticity of MgO and a primary pressure scale to 55 GPa, *Proc. Natl. Acad. Sci. USA* **97**, 13494-13499.

90. Merkel, S., Wenk, H.-R., Shu, J.F., Shen, G.Y., Gillet, P., Mao, H.K., Hemley, R.J. (2002) Deformation of polycrystalline MgO at pressures of the lower mantle, *J. Geophys. Res.* **107**, art. 2271.

91. Liechtenstein, A.I., Anisimov, V.I., Zaanen, J. (1995) Density functional theory and strong interactions – orbital ordering in Mott-Hubbard insulators, *Phys. Rev.* **B52**, R5467-R5470.

92. Rohrbach, A., Hafner, J., Kresse, G. (2003) Electronic correlation effects in transition-metal sulfides, *J. Phys. : Condens. Matter* **15**, 979-996.

93. Szotek, Z., Temmerman, W.M., Winter, H. (1993) Application of the self-interaction correction to transition-metal oxides, *Phys. Rev.* **B47**, 4029-4032.

94. Becke, A.D. (1993) Density-functional thermochemistry. 3. The role of exact exchange, *J. Chem. Phys.* **98**, 5648-5652.

95. Bredow, T. and Gerson, A.R. (2000) Effect of exchange and correlation on bulk properties of MgO, NiO, and CoO, *Phys. Rev.* **B61**, 5194-5201.

96. Aryasetiawan, F. & Gunnarsson, O. (1998) The GW method, *Rep. Prog. Phys.* **61**, 237-312.

97. Foulkes, W.M.C., Mitas, L., Needs, R.J., & Rajagopal, G. (2001) Quantum Monte Carlo simulations of solids, *Rev. Mod. Phys.* **73**, 33-83.

98. Kohn, W., Meir, Y., Makarov, D.E. (1998) Van der Waals energies in density functional theory, *Phys. Rev. Lett.* **80,** 4153-4156.

99. Fuchs, M. and Gonze, X. (2002) Accurate molecular properties from density-functional theory : the adiabatic-connection fluctuation-dissipation approach, *Phys. Rev.* B **65**, art. 235109.

100. Iitaka, T. & Ebisuzaki, T. (2001) First-principles calculation of elastic properties of solid argon at high pressures, *Phys. Rev.* **B65**, art. 012103.